Research Square

Preprints are preliminary reports that have not undergone peer review.
They should not be considered conclusive, used to inform clinical practice,
or referenced by the media as validated information.

# Study on seismic performance of cold-formed thin-walled steel composite walls infilled with fiber gypsum-embedded straw bricks

**Kangle Ren**
Lanzhou University of Technology
**Xiaolin Cao**
xlcao@lut.edu.cn

Lanzhou University of Technology
**Xiaodong Li**
Lanzhou University of Technology

**Article**

**Keywords:** cold-formed thin-wall steel composite wall; embedded straw bricks; fibrous gypsum; pseudo-static test; seismic performance

**Posted Date:** November 12th, 2026

**DOI:** https://doi.org/10.21203/rs.3.rs-11413181/v1

**License:** This work is licensed under a Creative Commons Attribution 4.0 International License.
Read Full License

**Additional Declarations:** No competing interests reported.

**Study on seismic performance of cold-formed thin-walled steel composite walls infilled with fiber gypsum-embedded straw bricks**

Kangle Ren[1]; Xiaolin Cao[1]; Xiaodong Li[1]

[1]School of Civil and Hydraulic Engineering , Lanzhou University of Technology, Lanzhou 730050, China.

**Corresponding author**: Xiaolin Cao. **Tel.**:18662715722, **E-mail:** xlcao@lut.edu.cn

**Acknowledgments**

The work was supported by the National Natural Science Foundation of China (Grant No. 51968043).

**Abstract**

To reduce the self-weight of infilled cold-formed thin-walled steel composite walls and improve their strength, stiffness and seismic performance, this paper presents a composite wall configuration with embedded straw bricks. Three groups of full-scale specimens were fabricated and subjected to low-cyclic reversed loading tests. The failure modes, hysteretic responses, skeleton curves, ductility, stiffness degradation and energy dissipation capacity were systematically analysed to reveal how structural configurations affect the seismic behaviour of the walls. Test results show that wall failure is mainly characterised by gypsum cracking, while straw bricks suffer negligible damage. The proposed system effectively upgrades the bearing capacity, lateral stiffness and ductility of infilled cold-formed thin-walled steel composite walls. Relative to hollow walls, the bearing capacity increases by 377.5%, lateral stiffness by 34.6%, and the ductility coefficient by 226.8%. The flat steel strip frame alleviates gypsum board damage and exhibits excellent ductility, whose ductility coefficient is 111% higher than hollow walls. In addition, the ductility coefficient of the straw-brick-embedded composite wall is 54.6% greater than that of the flat steel strip light steel frame wall.

**Key words:** cold-formed thin-wall steel composite wall; embedded straw bricks; fibrous gypsum; pseudo-static test; seismic performance

## 1. Introduction

Against the background of continuous innovation in green energy-efficient buildings, China has strengthened carbon emission reduction and promoted construction industrialization, and green construction philosophies have gained wider application. [1]. Therefore, the development of prefabricated buildings is of great significance for improving construction quality, accelerating construction schedules and advancing sustainable development. [2]. As a typical green prefabricated building system, cold-formed thin-walled steel residential structures have undergone extensive development and wide application in China in recent years.

Cold-formed thin-walled steel composite walls act as the main load-bearing and lateral force-resisting components of such structural systems. Using full-scale experiments, numerical simulations and theoretical analyses, scholars worldwide have conducted extensive research on the sheathing effect of wall panels, together with the shear, seismic and axial compressive performance of composite walls [3,4]. To improve the lateral stiffness of cold-formed thin-walled steel composite walls, researchers worldwide firstly investigated the application of cladding panels [5,6] and bracing systems [7,8]. Mohebbi et al. [9] performed experimental tests on cold-formed thin-walled steel composite walls with single-sided and double-sided claddings consisting of steel plates, cement fibre boards and gypsum boards. Their results indicated that the shear stiffness and energy dissipation capacity of walls with double-sided cladding increased by 63% and 70%, respectively, relative to those with single-sided cladding. Zhou et al. [10] adopted the finite element method to analyse the effects of various wall sheathing materials on the bearing capacity of composite walls. Numerical simulations and parametric analyses indicated that cladding materials exert a remarkable influence on the shear capacity of composite walls. Shi et al. [11,12] utilised ABAQUS to numerically investigate the hysteretic behaviour of diagonal bracings in supported cold-formed thin-walled steel composite walls. Yuan et al. [13] proposed a cold-formed thin-walled steel composite wall equipped with Z-shaped bracings. On the basis of experimental tests and finite element analyses, they explored the effects of such bracings on wall shear performance. The results revealed that Z-shaped bracings substantially improve the shear performance of composite walls compared with hollow frame walls.

In recent years, driven by the popularization of green energy-saving materials, researchers worldwide have carried out investigations on cold-formed thin-walled steel composite walls infilled with lightweight materials [14–17]. Pakizeh et al. [18] and Hegyi et al. [19] developed a composite wall system consisting of cold-formed steel frames infilled with polystyrene concrete, and experimental tests were implemented to assess its mechanical behaviour. The test results show that, in comparison with double-sheathed cold-formed thin-walled steel hollow walls, internal lightweight infills effectively increase wall stiffness, stability and bearing capacity, and restrain deformation and buckling. Fang et al. [20] studied the compressive and shear behaviour of cold-formed thin-walled steel–foamed concrete composite walls, and verified that foamed concrete infill substantially improves the shear stiffness, ductility and energy dissipation capacity of composite walls. Xu et al. [21] proposed an innovative composite wall composed of cold-formed thin-walled steel and high-strength foamed concrete, which exhibited favourable ductility and energy absorption performance. Wu C et al. [22] compared the seismic behaviour of cold-formed thin-walled C-channel steel frames and composite walls double-clad with fire-resistant straw panels. The results proved that the double-sided straw panel composite wall possesses remarkably higher bearing capacity and superior seismic performance. Hu et al. [23,24] put forward a novel phosphogypsum-infilled cold-formed thin-walled steel composite wall and conducted combined experimental and numerical analyses. This innovative configuration greatly improves the shear resistance and seismic performance of conventional CFS walls. Wu et al. [25] explored the seismic behaviour of cold-formed thin-walled steel composite walls infilled with lightweight desulfurized gypsum modified materials, and confirmed that infilling significantly enhances the shear capacity and lateral stiffness of composite walls. Chen et al. [26] performed full-scale experimental tests on cold-formed thin-walled steel composite walls with and without gypsum-based composite infills. Their test results indicate that the axial compressive capacity of infilled composite walls is 1.8–2.9 times that of unfilled walls, and the magnitude of bearing capacity improvement is closely related to the strength and density of gypsum-based fillers.

However, the popularization of cold-formed thin-walled steel composite walls currently encounters two major

obstacles. First, as cold-formed thin-walled steel buildings develop toward multi-storey configurations, the height and self-weight of composite walls increase, which aggravates seismic responses at each floor and limits the further application of such structural systems. Second, influenced by the centuries-long traditional architectural culture of "Qin bricks and Han tiles", the public tends to favour conventional construction forms, creating resistance to the adoption of innovative composite wall structures.

This work adopts embedded plant straw bricks to lower the self-weight of composite walls, and lightweight gypsum composites as infills to avoid hollow cavities between double-sided wall sheathing. Accordingly, aiming to improve wall stiffness and seismic performance, reduce self-weight and eliminate the hollow drum effect induced by inter-panel cavities, this paper proposes an innovative cold-formed thin-walled steel composite wall infilled with light gypsum embedded straw bricks and covered with gypsum boards on both sides, as illustrated in Figure 1. Pseudo-static tests under low-cyclic horizontal loading were carried out to explore the failure mechanism and seismic behaviour of the proposed wall. The research outcomes can support subsequent theoretical studies and engineering applications of composite walls of this type, and lay a basis for developing other novel infill materials for cold-formed thin-walled steel composite walls.

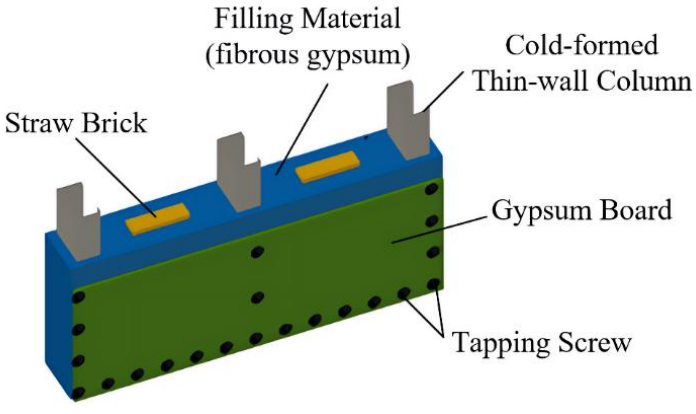



**Fig.1** Fiber gypsum embedded straw bricks filled cold-formed thin-wall steel composite wall

## 2. Test Overview

### 2.1 Specimen Design

According to the test methods suggested in JGJ 227-2011 *Technical Regulations for Construction of Low-Rise Cold-Formed Thin-Walled Steel Houses* [27], three full-scale specimens of cold-formed steel composite walls were designed and fabricated. The specific parameters are detailed in Table 1.

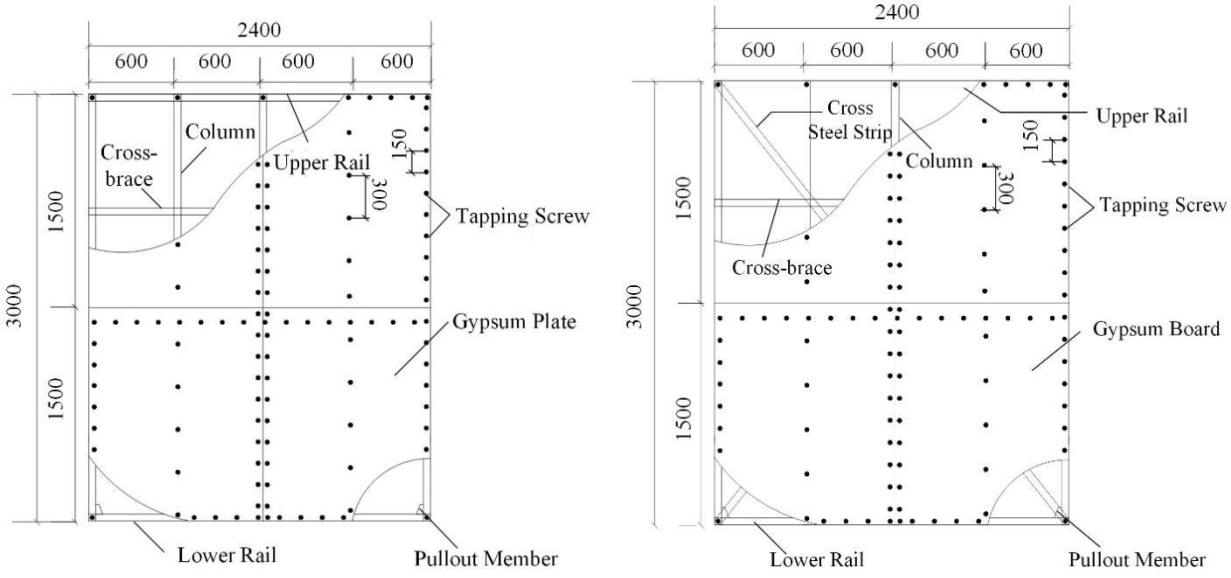
**Table 1** Design parameters of composite wall

| Specimen number | Specimen height width（m） | Filler plaster | Built-in straw brick | Arrange the cross-steel strips |
|---|---|---|---|---|
| W-1 | 3.0m×2.4m | No | No | No |
| W-2 | 3.0m×2.4m | No | No | Yes |
| W-3 | 3.0m×2.4m | Yes | Yes | No |

The wall specimens have dimensions of 3000 mm × 2400 mm (height × width). Vertical studs are arranged at a spacing of 600 mm and adopt C-shaped cold-formed thin-walled steel sections with a specification of C90×40×14×1.2 mm (web height × flange width × lip width × plate thickness). The two boundary studs at both ends of each wall are I-shaped built-up sections formed by back-to-back assembled C-shaped steel members, fastened by double rows of screws at 300 mm spacing. The top and bottom tracks and cross bracings are fabricated from U-shaped cold-formed thin-walled steel (U93×35×1.2 mm; web height × flange width × lip width). All specimens are clad with 12 mm-thick gypsum boards sized 1500 mm × 1200 mm (length × width). ST4.8 round-head self-tapping screws are adopted for connections between studs, tracks and internal steel strips, whereas ST4.2 flat-head self-tapping screws are used to attach wall panels to steel frames. The screw spacing is 150 mm along panel peripheries and 300 mm in the interior regions. Specimen W-2 is equipped with 50 mm-wide and 1.2 mm-thick horizontal steel strips. For specimen W-3, one layer of gypsum board was installed first, followed by staged gypsum casting. Straw bricks were embedded after one-third of the gypsum pouring was completed. The straw bricks were manufactured by mixing plant straw, ramie fiber, soil, fly ash and glutinous rice glue in predetermined proportions and compacting the mixture in 300 mm × 300 mm × 30 mm moulds. The finished straw bricks are presented in Figure 2. Subsequently, gypsum blended with two types of fibers was cast and cured. Detailed configurations of all specimens are shown in Figure 3.

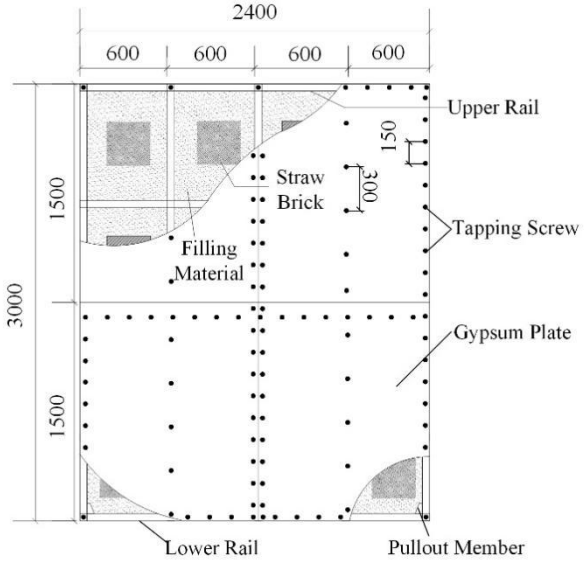


**Fig. 2** Straw brick test block




(a) Specimen W-1

(b) Specimen W-2




(c) Specimen W-3

**Fig. 3** Specimen geometry and structure

### 2.2 Material Properties

The steel frames of all wall specimens are constructed from cold-formed thin-wall steel galvanized sheets with a strength grade of Q235B and a base material thickness of 1.2 mm. In accordance with the relevant provisions of *Tensile Testing of Metallic Materials—Part 1: Test Method at Room Temperature* (GB/T 228.1-2010) [28], tensile specimen tests were conducted, and the material test results are presented in Table 2. The material properties of the straw bricks and gypsum are shown in Table 3.

**Table 2** Mechanical properties of galvanized steel sheet

| Thickness t/mm | Modulus of elasticity E/GPa | Yield strength $f_y$/ MPa | Tensile strength $f_u$/ MPa | Elongation $\delta$/% |
|---|---|---|---|---|
| 1.2 | 246 | 456.9 | 504.6 | 31 |

**Table 3** Properties of straw bricks and gypsum

| Material class | Density /(kg·m$^{-3}$) | Compressive strength /MPa | Modulus of elasticity /MPa |
|---|---|---|---|
| Straw brick | 470.3 | 6.12 | 13 |
| Gypsum | 898.4 | 4.79 | 188 |

### 2.3 Test Loading Scheme

The test was carried out on a self-designed loading frame in the Structural Laboratory of Lanzhou University of Technology, as shown in Figure 4. The bottom track of the specimen was connected to the base beam, which was anchored to the laboratory floor. The top track was linked to the top beam for the application of horizontal and vertical loads. Diagonal bracings were arranged on both sides of the composite wall to restrain out-of-plane instability. The vertical load was determined according to the load borne by the bottom wall of a three-storey building. Referring to Technical Specification for Thin-Walled Tubular Girder Light Steel Buildings (DBJ/CT 045-2008) [29], a vertical load of 30 kN was uniformly applied on the wall top track to simulate the load of the ground floor. Horizontal load was exerted via a 100 kN MTS hydraulic actuator with a loading rate of 1 mm/s. Real-time data were acquired by the actuator control system to obtain the hysteretic curves in post-processing. A displacement-controlled loading scheme consisting of two phases was adopted. Before yielding, single-cycle loading was implemented with an incremental displacement

of 1.5 mm per level. After yielding, the displacement increment was increased to 8 mm, and three repeated loading cycles were performed at each displacement level. The loading protocol is presented in Figure 5. The damage evolution of composite walls was continuously recorded throughout the test.

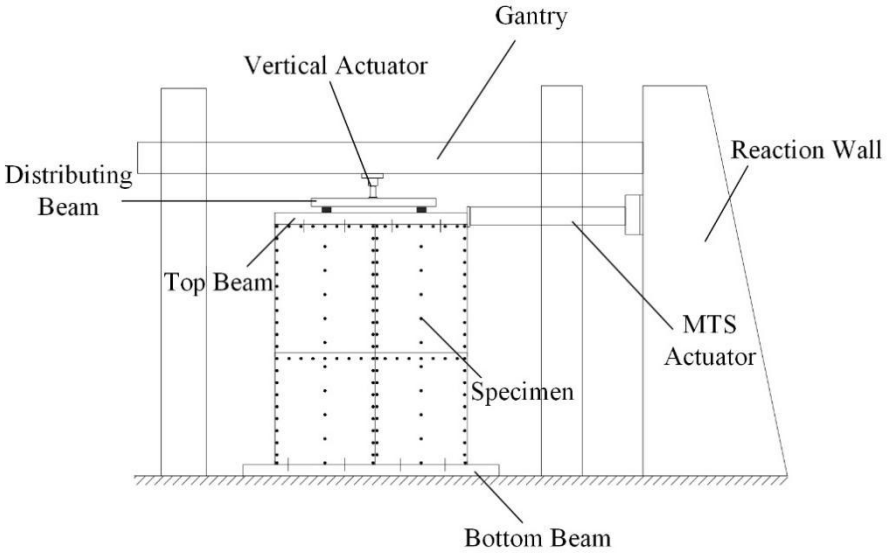



**Fig. 4** Test device

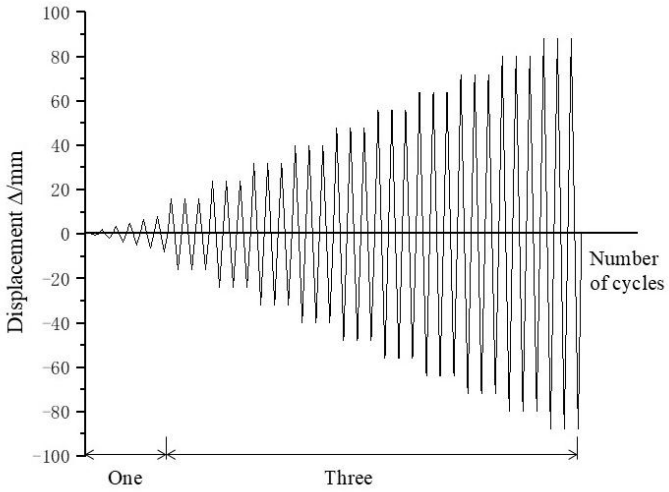



**Fig. 5** Loading system

### 2.4 Point Arrangement

Displacement transducers were arranged as illustrated in Figure 6 to acquire the shear deformation of the composite walls. Specifically, D1 and D2 measured the horizontal displacements of the loading top beam and specimen top, respectively. D3 recorded the relative horizontal displacement between the specimen bottom and the base beam. D4 and

D5 captured the vertical displacement of the specimen relative to the base beam, while D6 and D7 monitored the vertical displacement of the base beam with respect to the ground. In addition, D8 was deployed to measure the horizontal displacement of the base beam relative to the ground.

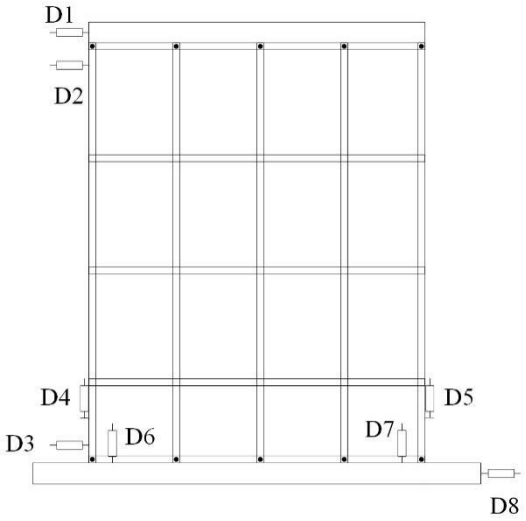
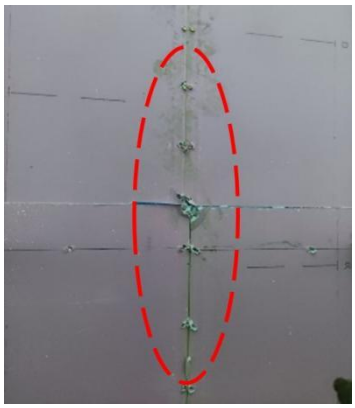



**Fig. 6** Displacement meter arrangement

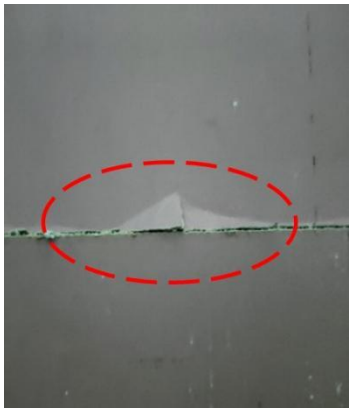
## 3. Test Phenomena and Failure Characteristics

### 3.1 Specimen W-1

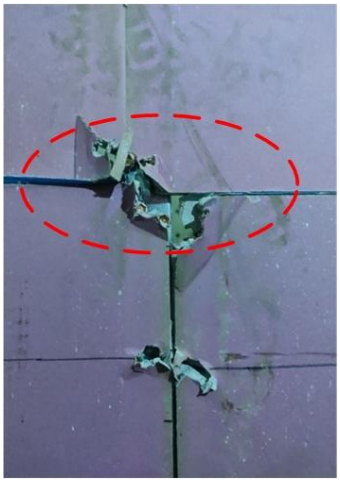
The failure of specimen W-1 was dominated by gypsum board damage, while the steel skeleton remained intact without evident damage. At a displacement of 40 mm, screws around the gypsum board began to tilt, accompanied by gradual enlargement of screw holes. Continuous displacement loading further widened the gaps between adjacent gypsum boards. When the displacement increased to 64 mm, peeling failure occurred at the four corners and splicing joints of the gypsum board. Upon further loading to 80 mm, the gypsum board screws were pulled out, causing significant dislocation of the gypsum boards and eventual failure of the wall sheathing effect. The typical failure mode of specimen W-1 is presented in Figure 7.



(a) The screw was tilted and the screw hole became larger



(b) Gypsum board peeling



(c) Evident misalignment of the gypsum board



(d) Bottom screw pulled out

**Fig. 7** Failure mode of W-1

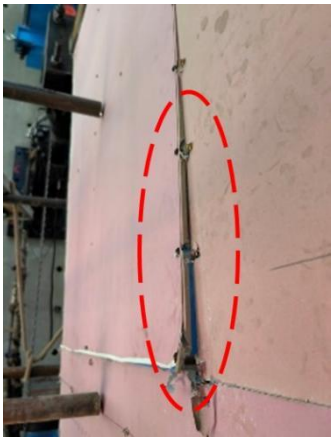
### 3.2 Specimen W-2

Specimen W-2 was modified by attaching cross steel strips to one side of the light steel skeleton. Affected by the diagonal compression strut mechanism, the screws at the middle of the cross steel strips were firstly pulled out when the lateral displacement reached 32 mm. At a displacement of 48 mm, the upper cross steel strips completely detached, accompanied by slight dislocation at the gypsum board joints. As the displacement increased to 64 mm, partial screw pull-out occurred at the lower cross steel strips, and local warping appeared at the gypsum board joints. When the displacement further increased to 80 mm, the lower cross steel strips failed and lost their bearing capacity, and the screws at the gypsum board joints began to withdraw. At the ultimate displacement of 88 mm, peripheral screws of the gypsum board were pulled out and middle screws tilted, whereas the steel skeleton still

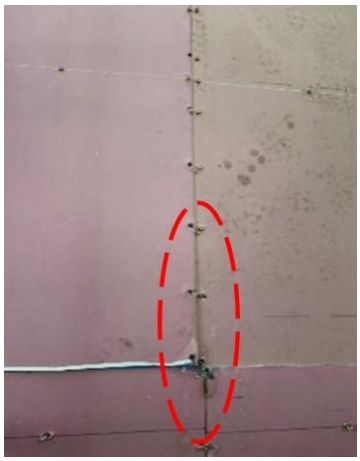
sustained no obvious damage. Compared with specimen W-1, W-2 exhibited milder screw damage, as the cross steel strips effectively shared part of the lateral load at the early loading stage. The typical failure modes of specimen W-2 are illustrated in Figure 8.



(a) The screws at the joint were removed



(b) Gypsum board peeling



(c) The screws at the joint were removed



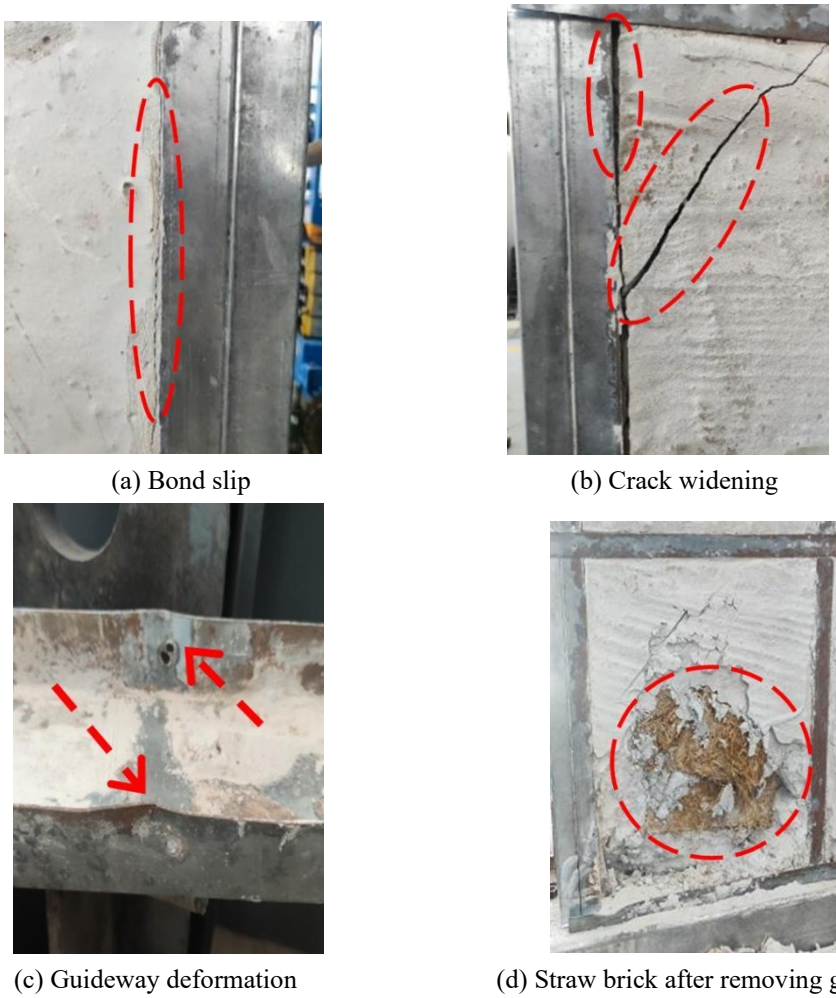
(d) Gypsum board peeling

**Fig. 8** Failure mode of W-2

### 3.3 Specimen W-3

For specimen W-3, no visible damage to the infill material was detected at the initial loading stage. When the lateral displacement reached 16 mm, interfacial slip and debonding took place between the gypsum infill and vertical studs. With continuous loading, such slip became prominent, and gaps gradually formed between the infill and steel skeleton, whereas no cracks emerged at the interfaces between straw bricks and gypsum. At a displacement of 40 mm, cracks initiated on the right side of the bottom gypsum infill. When the displacement increased to 56 mm, cracks propagated

within gypsum infill blocks and extended towards the embedded straw bricks; meanwhile, gypsum infill at the upper corner crushed and spalled. Upon further loading to 72 mm, crack widths enlarged, the internal infill lost integrity, and surface gypsum boards started to crack. The test was terminated at a displacement of 80 mm due to the remarkable degradation observed in the hysteretic curves. At this stage, pull-out failure of gypsum board screws occurred, leading to separation between gypsum boards and the steel skeleton. After stripping away the infill material, slight deformation was found in the bottom track of the light steel frame, while the embedded straw bricks remained nearly intact. The typical failure modes of specimen W-3 are presented in Figure 9.



(a) Bond slip (b) Crack widening

(c) Guideway deformation (d) Straw brick after removing gypsum

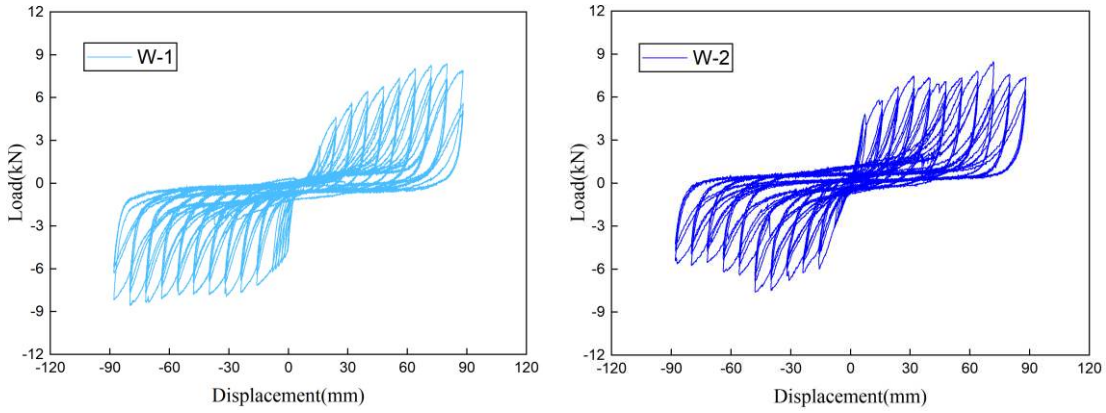
**Fig. 9** Failure mode of W-3

## 4. Analysis of Test Results

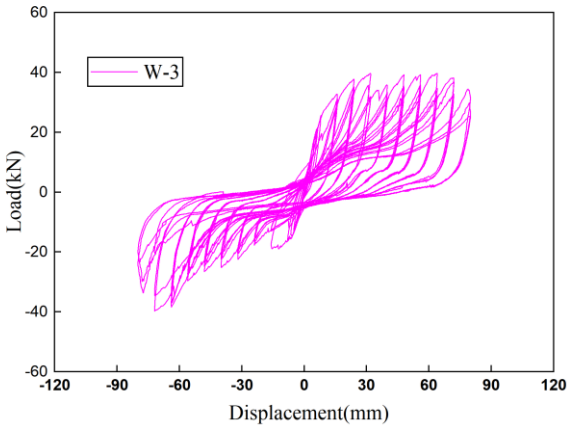
### 4.1 Hysteresis Curve

The load–displacement hysteretic curves of all specimens are plotted in Figure 10. At the initial loading stage, the

three specimens exhibited fusiform hysteretic curves. With increasing displacement, obvious slip developed in specimen W-1, giving rise to severe pinching and transforming the curve into a Z shape. This phenomenon can be attributed to extrusion damage at panel joints under amplified displacement, which induced dislocation and pull-out of self-tapping screws; consequently, the gypsum boards lost their restraint effect on the steel skeleton. Compared with W-1, specimen W-2 displayed weaker pinching behaviour. The cross steel strips offered extra restraint to the light steel frame and alleviated damage to self-tapping screws and wall panels. Meanwhile, W-2 maintained favourable ductility after yielding. Nevertheless, its hysteretic curve gradually evolved into a Z shape in the late loading stage once the cross steel strips and gypsum boards failed. Specimen W-3 achieved substantially higher bearing capacity, yet moderate pinching appeared in the mid-loading phase due to interfacial slip and progressive deterioration of the gypsum infill. An evident drop in bearing capacity was observed at a displacement of 40 mm, originating from the loosening of bolts connecting the frame and base beam. Unlike W-1 and W-2, W-3 showed negligible slip in the later loading period. The fractured gypsum infill together with undamaged embedded straw bricks still provided partial support for the steel skeleton, contributing to much fuller hysteretic loops.




(a) Specimen W-1 (b) Specimen W-2




(c) Specimen W-3

**Fig. 10** Hysteresis curves of each specimen

### 4.2 Skeleton Curve

The skeleton curves of specimens W-1, W-2, and W-3 are illustrated in Figure 11.

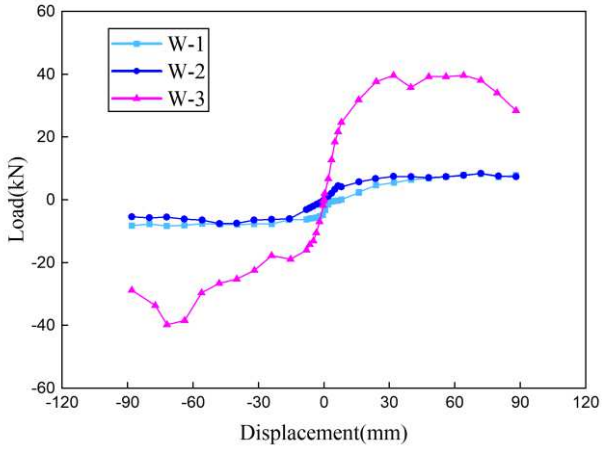



**Fig. 11** Skeleton curves of each specimen

As shown in Figure 11, the peak load-bearing capacity of W-3 is 4.77 times that of W-1, while the peak load-bearing capacity of W-2 is similar to that of W-1. This indicates that, compared to changing the structure of the light steel frame, the fiber gypsum embedded straw brick infill wall can effectively improve the bearing capacity. During the initial loading stage, the load-bearing capacity of W-2 exceeds that of W-1 due to the diagonal bracing provided by the cross-steel strips. After reaching the peak load, both W-2 and W-1 exhibit peak platforms, but the platform for W-2 is wider than that of W-1, indicating that the addition of cross steel strips enhances the wall's ductility. Under the reciprocating

load, the W-3 curve and the positive and negative skeleton curves of the specimen exhibit noticeable asymmetry. This asymmetry arises because the block-by-block filling method used during the gypsum filling process affects the performance of the gypsum filler, leading to variations between each block. Additionally, the embedded straw bricks contribute to the asymmetric curve phenomenon due to differences in various aspects. However, after W-3 reaches its peak load, the load gradually decreases with increasing displacement, indicating that the W-3 specimen also demonstrates good ductility.

### 4.3 Ductility Property

The ductility coefficient reflects the deformation capacity of structural members and serves as a critical indicator for evaluating the seismic performance of structures. In this test, the ductility coefficient was calculated in accordance with the provisions of the *Seismic Test Code for Buildings* (JGJ/T101-2015) [30]. The expression is as follows:

$$\mu = \frac{\Delta_u}{\Delta_y} \tag{1}$$

Here, $\Delta_u$ represents the ultimate displacement of the specimen, and $\Delta_y$ denotes the yield displacement of the specimen. The calculation results are summarized in Table 4.

**Table 4** Characteristic values of skeleton curves of each specimen

| Specimen number | Yield load $P_y$/kN | Yield displacement△ $_y$/mm | Peak load $P_{max}$/ kN | Peak displacement △$_{max}$/mm | Ultimate load $P_u$/kN | Ultimate displacement△ $_u$/mm | Ductility coefficient μ |
|---|---|---|---|---|---|---|---|
| W-1 | 7.3 | 52.1 | 8.30 | 71.98 | 7.06 | 78.01 | 1.49 |
| W-2 | 7.1 | 27.34 | 8.45 | 71.89 | 7.18 | 86.03 | 3.15 |
| W-3 | 33.1 | 16.32 | 39.63 | 63.97 | 33.69 | 79.48 | 4.87 |

As shown in Table 4, due to the damage of self-tapping screws, the panel of specimen W-1 loses the skin effect, resulting in a rapid decline in bearing capacity and poor ductility performance. However, compared with specimen W-1, the ductility coefficient of specimen W-2 increased by 1.85 times. This indicates that the light steel skeleton with

diagonal brace structure has better ductility. The main reason is that the cross-steel strip weakens the damage of tapping screws and reduces the yield displacement of specimens. Compared with W-2, the ductility coefficient of W-3 is 54.6% higher, indicating that the specimen filled with fiber gypsum embedded straw bricks exhibits significantly better ductility than the light steel skeleton structure.

### 4.4 Stiffness Degradation

Stiffness degradation significantly impacts the performance of shear walls, making it a critical consideration in the construction industry. In this study, the secant stiffness *K* is employed to characterize the stiffness degradation behavior of the wall. Figure 12 shows the stiffness degradation curves of each specimen.

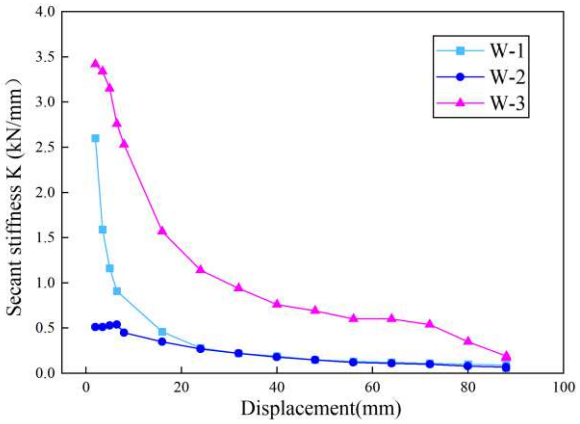



**Fig. 12** Stiffness degradation curves of each specimen

As can be seen from Figure 12, the stiffness degradation of W-1 and W-2 is rapid during the initial loading stage. However, the stiffness degradation of W-2 slows down and even exhibits an upward trend. This is because the cross-steel strip was not fully tightened at the initial loading stage, and as the horizontal displacement increased, the stiffness of the specimen improved within a certain range. The initial stiffness of W-2 is lower than that of W-1, indicating that the horizontal cross steel strip does not enhance the lateral stiffness of the specimen. However, the stiffness degradation amplitude of W-2 is smaller compared to W-1, suggesting that the horizontal cross steel strip effectively delays stiffness degradation and, to some extent, strengthens the wall's resistance to seismic forces. The initial stiffness of W-3 is 3.5kN/mm, which is 1.35 times that of the W-1 specimen. After the yield stage, the stiffness degrades slowly, indicating

that filling fiber gypsum and embedded straw bricks not only enhances the lateral stiffness but also mitigates stiffness degradation, thereby improving the seismic performance of the wall.

**4.5 Energy-consuming Capacity**

In accordance with the JGJ/T101-2015 *Building Seismic Test Code* [30], the energy dissipation capacity of the specimen is evaluated based on the area enclosed by the hysteresis loop. In this study, the cumulative dissipated energy $E$ is utilized to assess the energy dissipation capacity of the specimen.

Figure 13 illustrates the cumulative energy dissipation $E$ of all specimens during the first loading cycle at each stage. As shown in Figure 13, the cumulative dissipated energy of W-3 is significantly higher than that of W-2 and W-1, being 6.5 times and 7.04 times greater, respectively. This indicates that the filler and embedded straw bricks can absorb more energy during displacement loading by providing additional bracing to the frame, thereby significantly enhancing the energy dissipation capacity of the wall. The cumulative energy dissipation of W-2 is 1.1 times that of W-1, indicating that its effect on enhancing energy dissipation capacity is limited. This is primarily because the cross-steel strip was not fully tensioned during the initial loading stage, preventing the diagonal bracing function from being fully utilized. As a result, the energy dissipation contribution of the flat cross steel strip to the overall wall is diminished. The above data indicate that modifying the light steel skeleton structure with flat steel strips does not significantly enhance the energy dissipation effect. In contrast, embedding straw bricks within the filler can substantially improve the wall's energy dissipation capacity.

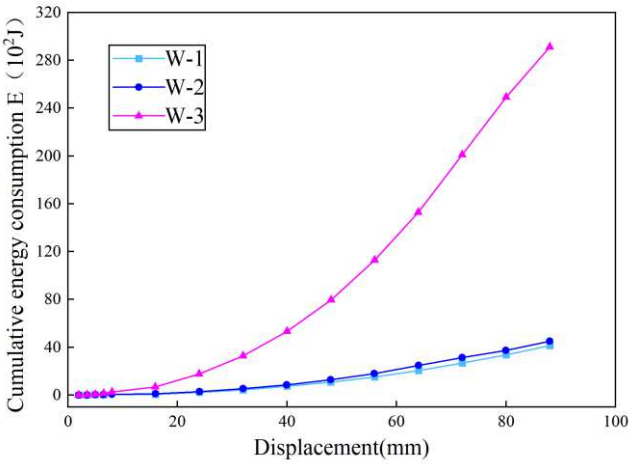



**Fig. 13** Cumulative energy dissipation curves of each specimen

## 5 Conclusions

Low-cyclic horizontal loading tests were carried out on three types of cold-formed thin-walled steel composite walls, including hollow walls, steel-strip-reinforced walls and fiber gypsum walls embedded with straw bricks. Based on observed failure phenomena and seismic performance indices, several key conclusions are drawn as follows:

(1) The dominant failure modes of the fiber gypsum composite wall infilled with embedded straw bricks are interfacial slip between gypsum infill and the light steel frame and cracking of the base gypsum, whereas the embedded straw bricks remain basically intact. For light steel frame composite walls equipped with horizontal cross steel strips, the cross strips detach firstly under the diagonal compression strut effect. Subsequent damage to panels and screws further causes the loss of wall sheathing effect.

(2) The fiber gypsum wall infilled with embedded straw bricks can effectively enhance the bearing capacity, lateral stiffness and ductility of cold-formed thin-walled steel composite walls. Compared with hollow composite walls, its bearing capacity increases by 377.5%, lateral stiffness by 34.6%, and ductility coefficient by 226.8%, which greatly improves the seismic performance of CFS composite walls.

(3) Optimizing the configuration of light steel frames by adding horizontal cross steel strips yields limited improvement in seismic behaviour. The bearing capacity and lateral stiffness experience no obvious enhancement, while the ductility coefficient rises by 111% relative to the conventional light steel frame wall, demonstrating improved

deformation capacity. By comparison, the specimen with fiber gypsum and embedded straw brick infill achieves better ductility performance, with an additional 54.6% increment in the ductility coefficient.

**Conflicts of Interest:** The authors declare that they have no conflict of interest.

**Data availability**

The datasets used and/or analysed during the current study are available from the corresponding author on reasonable request.

**References**


1. Alqahtani, F. K.: Development of Composite PET Plastic-based Aggregate and its Utilization in Green Lightweight Concrete. J. Arabian Journal for Science and Engineering. 47(10):13397-13406 (2022)
2. Liao, L.-P.: Development status and strategy of green prefabricated buildings. J. Journal of Enterprise Economics. 38 (12): 139-146 (2019)
3. Liu, X.-B.: Research on Lateral Force Resistance of cold-formed steel composite Wall filled with light materials based on gypsum. D. Chang 'an University, (2019)
4. Zhang, X.-H.; Ren, G.-S.; Zhang, E.-Y.: Experimental study on seismic performance of thin-walled steel-straw board composite walls with built-in steel plate. J. Journal of Building Engineering. 76 (2023)
5. Di, Y.-Q.; Zhang, Y.-X.; Li, G.-H.: Finite Element Analysis of Flexural Behaviour of Cold-formed Thin-Walled Steel Composite Wall for Building Cladding. J.IOP Conference Series: Earth and Environmental Science. 455012061-012061 (2020)
6. Wu, H.-H.; Sui, L.; Zhou, T.-H.: Estimation of lateral stiffness for gypsum-filled cold-formed steel shear walls. J. Structures. 32: 28-37 (2021)
7. Gao, W.-C.; Xiao, Y.: Review on shear performance of cold-formed thin-wall steel composite walls. J. Journal of Building Structures. 35(4): 30-40 (2014)
8. Blum, B. H.; Meimand, Z. V.; Schafer, W. B.: Flexural Bracing Requirements in Axially Loaded Cold-Formed Steel-Framed Walls. J. Practice Periodical on Structural Design and Construction. 20(4):04014043-04014043 (2014)
9. Mohebbi, S.; Mirghaderi, R.; Farahbod, F.: Experimental Work on Single and Double-Sided Steel Sheathed Cold-formed Steel Shear Walls for Seismic Actions. J. Thin-Walled structures. 91: 50-62 (2015)
10. Zhou, X.-H.; Shi, Y.; Zhou, T.-H.: Study on shear performance of cold-formed thin-wall steel composite wall. J. Journal of Building Structures. (03): 42-47 (2006)
11. Shi, Y.; Ran, X.-W.; Xiao, W.: Experimental and numerical study of the seismic behavior of cold-formed steel walls with diagonal braces. J. Thin-Walled Structures. 107318-. (2020)
12. Shi, Y.; Ran, X.-W.; Xiong, G.: Numerical modeling on shear performance of braced cold-formed steel composite walls. J. Journal of Constructional Steel Research. 198 (2022)
13. Yuan, Q.; Wang, Z.-H.; Yang, Y.: Research on shear resistance of cold-formed thin-wall steel grout wall with intermediate support. J. Journal of Hunan University (Natural Science Edition). 48(9): 108-117 (2021)
14. Karthika, S.; Lakshimikandhan, K. N.; Sivakumar, P.; Load Deflection Characteristics of Sustainable Infilled Concrete Wall Panels. J. Arabian Journal for Science and Engineering. 41(2):451-460 (2016)
15. Li, H.-X.; Liu, D.-Z.; Wu, S.-Y.: Research on load-bearing performance of cold-formed thin-wall steel-foam concrete composite wall. J. Industrial Building. 50(10):160-169 (2020)
16. Aziz I, Hassan Muhammad Irfan UI, Haq Ehsan UI.: Development of Geopolymer Foam Concrete Incorporating Sugarcane Bagasse Ash and Fly Ash; 100% Recycled and Cement-Less Concrete. J. Arabian Journal for Science

and Engineering. 48(4):5655-5665 (2022)
17. Gao, H.-F.; Pan, Z.-H.; Zhu, W.-B.: Seismic Performance of Cold-Formed Thin-Walled Steel-Composite Shear Wall with Double-Layer Inclined Slots and Stiffeners. J. International Journal of Civil Engineering.1-20 (2025)
18. Pakizeh, M. R.; Parastesh, H.; Hajirasouliha, I.: Seismic performance of CFS shear wall systems filled with polystyrene lightweight concrete: experimental investigation and design methodology. J. Steel and Composite Structures. 46(4):497-512 (2023)
19. Hegyi, P.; Dunai, L.: Experimental study on ultra-lightweight-concrete encased cold-formed steel structures part II: stability behavior of elements subjected to compression. J. Thin-Walled Structures. 101:100-108 (2016)
20. Fang, H.-J; Qian, Z.-H.; Yao, B.: Experimental studies on the mechanical behaviors of cold-formed thin-walled steel-foam concrete composite walls. J. Advances in Structural Engineering. 27(9):1477-1489 (2024)
21. Xu, Z.-F.; Chen, Z.-F.; Osman, B.H.: Seismic performance of high-strength lightweight foamed concrete-filled cold-formed steel shear walls. J. Journal of Constructional Steel Research. 143:148-161 (2018)
22. Wu, C.; Sun, K.-F.; Chen, X.-H.: Seismic performance of cold-formed thin-walled C-shaped steel composite wall with fireproof straw boards cladding. J. Australian Journal of Structural Engineering. 25(3):278-294 (2024)
23. Hu, S.; Chen, Z.-P.; Ke, X.-J.: Numerical study on the seismic performance of phosphogypsum-filled cold-formed thin-walled steel composite walls. J. Thin-Walled Structures. 201(PA):111982-. (2024)
24. Hu, S.; Zhou, L.; Huang, Y.: Experimental investigation on the seismic performance of phosphorgypsum-filled cold-formed thin-walled steel composite walls. J. Thin-Walled Structures. 186 (2023)
25. Wu, H.-H.; Chao, S.-S.; Liu, X.-B.: Experimental Study on seismic Performance of cold-formed steel Composite Wall filled with light desulfurization gypsum modified material. J. Journal of Building Structures. 41(1): 42-50 (2020)
26. Chen, J.-W.; Fan, K.; Gao, L.: Experimental Study on axial compression Performance of cold-formed steel Composite Wall filled with gypsum Matrix Composite. J. Building Science. 34 (07): 48-53 (2018)
27. Technical Code for construction of low-rise cold-formed thin-wall steel buildings: JGJ 227-2011 [S]. Beijing: China Architecture and Construction Press (2011)
28. Tensile tests for metallic materials: Part 1: Test method at room temperature: GB/T 228. 1 -- 2010 [S]. Beijing: Standards Press of China (2010)
29. Shanghai Metal Structure Association. Technical specification for light steel with thin wall tube stringer: DBJ/CT 045-2008 [S]. Shanghai Building Materials Industry Market Management Station (2008)
30. Ministry of Housing and Urban-Rural Development of the People's Republic of China. Code of seismic test for buildings: JGJ/ T101-2015 [S]. Beijing: China Building and Construction Press (2015).